An hybrid-exchange density functional study of the bonding and electronic structure in bulk $CuFeS_2$.

Ruth Martínez-Casado,[1] Vincent H.-Y. Chen,[2] Giuseppe Mallia,[3] and Nicholas M. Harrison[3]

[1)] *Departamento de Fiscia Teórica de la Materia Condensada, Universidad Autónoma de Madrid, ES-28049 Madrid, Spain*

[2)] *Department of Physics, Imperial College London, South Kensington, London SW7 2AZ, United Kingdom*[a)]

[3)] *Thomas Young Centre, Department of Chemistry, Imperial College London, South Kensington London SW7 2AZ, UK*

(Dated: 17 March 2016)

The geometric, electronic and magnetic properties of bulk chalcopyrite $CuFeS_2$ have been investigated using hybrid-exchange density functional theory calculations. The results are compared with available theoretical and experimental data. The theoretical description of the bonding and electronic structure in $CuFeS_2$ is analyzed in detail and compared to those computed for chalcocite (CuS_2) and greigite (Fe_3S_4). In particular, the behavior of the $3d$ electrons of Fe^{3+} are discussed in terms of the Hubbard-Anderson model in the strongly correlated regime and found to be similarly described in both materials by an on-site Coulomb repulsion (U) of ~8.9 eV and a transfer integral (t) of ~0.3 eV.

[a)] vincent.chen08@imperial.ac.uk

I. INTRODUCTION

The I-III-VI subclass of chalcopyrite compounds ($A^{\rm I}B^{\rm III}X_2^{\rm VI}$) has drawn significant interest as the electrical, optical and structural properties, and in particular the band gap, can be engineered by altering the constituent elements or via doping[1]. Consequently, these compounds have found use in a range of semiconductor applications, such as non-linear optical devices[2,3], photodiodes[4,5], spintronic devices[6,7], and more recently, thin film intermediate band solar cells[8]. Copper-iron-sulfide chalcopyrite ($CuFeS_2$) is also commercially the most important copper ore as it accounts for the majority of copper reserves. The optimization of acid leaching chemistry for extracting copper from $CuFeS_2$ is becoming an important goal as processing ores of lower copper concentration becomes a necessity[9]. A detailed understanding of the structure, bonding, magnetic and electronic structure of $CuFeS_2$ is thus of significant current interest.

$CuFeS_2$ crystallizes in a tetragonal structure with space group $I\bar{4}2d(D_{2d}^{12})$[10] and exhibits a phase transformation to a cubic phase at around 800K[11]. The tetragonal phase, relevant to this study, consists of corner sharing M-S_4 tetrahedra arranged to produce atomic layers, parallel to the crystallographic a, b plane, of S and Cu/Fe composition and alternating along the crystallographic c direction. Spin moments are localized on the Fe-ions and coupled ferromagnetically within the metal layer and antiferromagnetically between layers resulting in a Nèel transition from the antiferromagnetic to paramagnetic state at 823 K[12]. The magnetic moment per Fe-ion deduced from neutron diffraction, is 3.85 $\mu_{\rm B}$ and is oriented along the crystallographic c-axis[13]. This is substantially lower than the magnetic moment characteristic of an isolated high-spin trivalent Fe^{3+} iron with d^5 configuration ($\mu_{\rm B} = 5$). In order to explain the low effective magnetic moment, it has been suggested that $CuFeS_2$ is a mixture of two ionic states, that is, $Cu^{+}Fe^{3+}(S^{2-})_2$ and $Cu^{2+}Fe^{2+}(S^{2-})_2$ [10,14]. Attempts to measure the optical (E_o) and fundamental (E_g) band gaps have lead to no clear consensus: the values of E_g obtained from infra-red absorption are in the range of 0.33-0.6 eV[15,16], while a value of 2.6 eV is derived from conductivity measurements using the four point method[17].

On the theoretical side the local density approximation (LDA) to density functional theory (DFT) was used to compare the electronic structure of $CuFeS_2$ to that of sphalerite, (Zn,Fe)S, and pyrite, FeS_2[18]. In this study the well known failings of the LDA led to $CuFeS_2$ being described as a non-magnetic metal. The generalized gradient approximation

(GGA) to DFT has been used to calculate phonons, elastic constants and thermodynamical properties[19] and to compare the electronic structure of the bulk to that of the (001) surface[20]. In these studies the calculated band gap is found to be indirect and very small (0.1 eV) and the discrepancy with that observed accredited to the fact that experiments are performed in defective or modified materials[20]. It is apparent that the electronic structure and physical properties of $CuFeS_2$ are sensitive to the correct treatment of on-site electronic interactions for which the LDA and GGA are not reliable approximations[21]. Further experimental studies of the electrical, optical, and magnetic properties as well as the results of electronic structure calculations have been compiled and discussed in a review by Nikiforov[22].

Compared to LDA and GGA, hybrid-exchange density functionals such as the Becke three parameter (exchange), Lee-Yang-Parr (correlation) functional (B3LYP), provide a more accurate description of the electronic structure of localized and strongly interacting systems that are non-conducting due to partial correction of electronic self-interaction. More recently, Conejeros *et al.* used B3LYP to investigate the electronic and magnetic properties of $CuFeS_2$[23]. They concluded that copper atoms behave diamagnetically in the range 170-300 K and that this was not due to partial oxidation but because of magnetic excitations on Fe spins which increase the amount of spin delocalization on neighbouring CuS_4 tetrahedra. The B3LYP is also employed in the current work with the aim of documentiing qualitatively correct and reliable electronic structure for the ground state of bulk $CuFeS_2$. The current work provids a deeper analysis of the electronic structure and the nature of the bonding in $CuFeS_2$. In particular, the Hubbard-Anderson model is used rationalize the electronic structure and the nature of the Cu-S and Fe-S bonds. This work will be the basis for future studies of the interaction of $CuFeS_2$ with the liquid state with the ultimate goal of understanding Cu dissolution and associated surface passivation mechanisms.

This article is organized as follows: Sec. II describes the computational method deployed. In Sec. III the geometry and electronic structure of the $CuFeS_2$ bulk ground state are presented and discussed along with a comparison with Cu_2S and Fe_3S_4. Finally, the main conclusions of this study are summarized in Sec. IV.

II. COMPUTATIONAL DETAILS

All calculations have been performed using the CRYSTAL09 software package[24], based on the expansion of the crystalline orbitals as a linear combination of a local basis set (BS) consisting of atom centered Gaussian orbitals. The BSs used for this work are all-electron BSs based on pre-existing ones from the literature. The BS for Cu was optimized by Doll and Harrison and used for their study of chlorine adsorption on the Cu(111) surface[25]. It consists of an 86-4111d(41) contraction [one s, five sp, and two d shell(s)]; the most diffuse $sp(d)$ exponents are α_{Cu}=0.150(0.392) Bohr^{-2}. The BS for Fe was based on the one employed by Catti *et al.* for their study of α-Fe_2O_3 (hematite)[26]. This BS has been adapted for this work by adding an additional diffuse sp shell consisting of a single Gaussian basis function with an appropriately chosen exponent so that the number of valence shells matches that of the Cu BS. The resulting BS, like the Cu BS, consists of an 86-4111d(41) contraction [one s, five sp, and two d shell(s)]; the most diffuse $sp(d)$ exponents are α_{Fe}=0.225(0.4345) Bohr^{-2}. The BS for S was optimized by Azavant and Lichanot and used for their study of Li_2S[27]. It consists of an 86-311d(1) contraction [one s, four sp, and one d shell(s)]; the most diffuse $sp(d)$ exponents are α_{S}=0.106(0.383) Bohr^{-2}.

Electronic exchange and correlation are approximated using the hybrid-exchange B3LYP functional[28,29], which has previously shown to provide a reliable ground state description of geometric parameters, band structures, and electronic and magnetic properties in a range of strongly correlated (mainly transition metal oxides) materials[30–37]. It has also been reported that the B3LYP functional reproduces the band gap of a wide range of materials including, semiconductors, sulfides and semi-ionic, ionic and transition metal oxides[21,38,39]. Matrix elements of the exchange and correlation potentials and the energy functional are integrated numerically on an atom-centered grid of points. The integration over radial and angular coordinates is performed using Gauss-Legendre and Lebedev schemes, respectively. A pruned grid consisting of 99 radial points and 5 sub-intervals with (146, 302, 590, 1454, 590) angular points has been used for all calculations (the XXLGRID option implemented in CRYSTAL09[24]). This grid converges the integrated charge density to an accuracy of about $\times 10^{-6}$ electrons per unit cell. The Coulomb and exchange series are summed directly and truncated using overlap criteria with thresholds of 10^{-7}, 10^{-7}, 10^{-7}, 10^{-7} and 10^{-14} as described previously[24,40]. Reciprocal space sampling was performed on a Pack-Monkhorst net

with a shrinking factor comparable to IS=4, which defines 14 symmetry unique k-points. The self consistent field procedure was converged up to a tolerance in the total energy of $\Delta E = 1 \cdot 10^{-7} E_h$ per unit cell.

The cell parameters and the internal coordinates have been determined by minimization of the total energy within an iterative procedure based on the total energy gradient calculated analytically with respect to the cell parameters and nuclear coordinates. Structural optimisation was performed using the Broyden-Fletcher-Goldfarb-Shanno (BFGS) scheme, as implemented in `CRYSTAL09`[24]. Convergence was determined from the root-mean-square (rms) and the absolute value of the largest component of the forces and displacements. The thresholds for the maximum and the rms forces (the maximum and the rms atomic displacements) have been set to 0.00045 and 0.00030 (0.00180 and 0.00120) in atomic units. Geometry optimization was terminated when all four conditions were satisfied simultaneously.

In order to gain further insight into the nature of bonding in $CuFeS_2$ and verify the $Cu^+Fe^{3+}(S^{2-})_2$ oxidation state, the geometric and electronic structure of $CuFeS_2$ has been compared with that of chalcocite (Cu_2S) and greigite (Fe_3S_4), chosen as from a formal charge point of view they contain ions in the same oxidation states, partially in the case of Fe_3S_4. For chalcocite, the monoclinic "low chalcocite" phase was considered in this work as this is the most stable phase under standard atmospheric conditions. The oxidation state of Cu_2S has been established as $(Cu^+)_2S^{2-}$, from the analysis of near-edge X-ray adsorption fine structure (NEXAFS) spectra obtained by Goh *et al.*[41]. Greigite, which has a spinel structure and a cubic unit cell, is believed to form from the oxidation of two thirds of Fe^{2+} cations in mackinawite ($Fe^{2+}S^{2-}$), in addition to rearrangement of the cubic S anion sublattice[42]. Greigite has two types of Fe sites; in each unit cell there are 8 tetrahedrally coordinated ferric (Fe^{3+}) cations (type A sites) and 16 octahedrally coordinated Fe that are a mixture of ferric (Fe^{3+}) and ferrous (Fe^{2+}) cations (type B sites)[43]. The structures of Cu_2S and Fe_3S_4 were optimized using the same numerical procedures and basis sets described above.

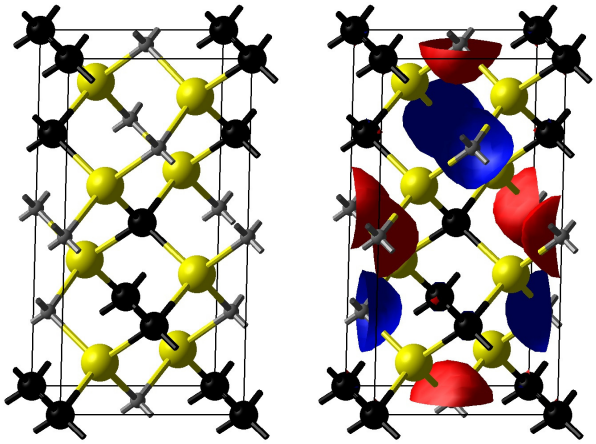
III. RESULTS

A. Geometry

Chalcopyrite ($CuFeS_2$) has a tetragonal unit cell of $I\bar{4}2d$ symmetry containing two Cu, two Fe and four S atoms. Optimizing the structure of $CuFeS_2$ by varying the cell and all internal coordinates while imposing $I\bar{4}2d$ symmetry results in the structure documented in Table I and visualized in Fig. 1a. Table I also includes lattice constants and bond lengths determined from previous DFT studies using various approximations for the electronic exchange and correlation including LDA[44] and GGA[19,44]. The table also presents experimental lattice constants deduced from X-ray diffraction on a natural single crystal specimens by Kratz *et al.*[45]. The tendency of LDA to overbind is well documented[39], however the underestimation of the lattice parameters by 5-6% reported by Zhou *et al.*[44] is significantly greater than what is typically observed for insulators (~1-2%). The lattice parameters estimated using the GGA functionals PBE and PW91, by Zhou *et al.*[44] and Łazewski *et al.*[19] respectively, provide a significant improvement on the estimated lattice constants. In the case of the latter, the estimated lattice parameters are unexpectedly close to the experimental ones. The general trend that GGA functionals tend to overcorrect the overbinding by LDA leading to the overestimation of lattice parameters for ionic insulators does not hold here[39,46,47]. For this work, the optimized lattice parameters differ slightly from experiment, with **a** and **c** overestimated by 3%. The discrepancy with experiment is due more to the overestimation of the Cu-S bond length (~4%) rather than the Fe-S bond length (~2%). The slight overestimation of lattice parameters and bond lengths is typical for ionic insulators when using the B3LYP functional[39,46]. This may in part be due to the neglect of London dispersion interactions.

B. Electronic Structure

In this section the electronic structure of $CuFeS_2$ is analyzed in terms of charges from Mulliken population analysis q, Born effective charges Z^*, the spin density and moments μ_B, the total and projected density of states and the band gap. The population analysis suggests ionic charges of $q_{Cu} = +0.483$, $q_{Fe} = +1.393$, and $q_S = -0.938|e|$, implying a semi-ionic model of bonding in $CuFeS_2$. However, charges obtained from Mulliken population



(a) Optimized bulk $CuFeS_2$ geometry.

(b) $CuFeS_2$ with spin density isosurfaces.

FIG. 1: The crystallographic cell for $CuFeS_2$ at the optimized geometry described in Table I. Large (yellow), medium (black) and small (gray) spheres correspond to the S, Cu and Fe atoms respectively. In the right panel (b) the spin density isosurfaces drawn at -0.005 (blue) and +0.005 (red) $|\mu_B|$/Bohr^3 illustrate the antiferromagnetic alignment of the Fe spins along the c-direction.

TABLE I: Optimized geometry for $CuFeS_2$ and comparison with previous theoretical results and experimental values obtained using X-ray diffraction. All quantities are in units of Angstroms. The percentage error of lattice constants and bond lengths relative to experiment are given in parentheses.

Param.	Expt.	LDA	GGA-PBE	GGA-PW91	Current work
a	5.286	4.955 (-6.3)	5.080 (-3.9)	5.265 (-0.4)	5.452 (3.1)
c	10.410	9.851 (-5.4)	10.003 (-3.9)	10.534 (1.2)	10.710 (2.9)
d_{Cu-S}	2.299			2.305 (0.3)	2.395 (4.2)
d_{Fe-S}	2.256			2.256 (0.0)	2.301 (2.0)
Ref.	45	44	44	19	

analysis are dependent on the choice of local basis set and so do not provide a definitive picture of the bonding. In Table II the Born effective charge tensors of Cu, Fe and S which were computed using the Berry phase method[48]. The Born effective charges of Cu, Fe, and

S, which correspond to 1/3 of the respective charge tensors are $Z^*_{\mathrm{Cu}} = 0.95$, $Z^*_{\mathrm{Fe}} = 2.96$ and $Z^*_{\mathrm{S}} = -1.97|e|$. These charges support a rather ionic model of the electronic structure of $CuFeS_2$ as $Cu^{+}Fe^{3+}(S^{2-})_2$. The Born charges computed using GGA-PW91 by Łazewski *et al.*[19] ($Z^*_{\mathrm{Cu}} = 0.75$, $Z^*_{\mathrm{Fe}} = 3.55$, and $Z^*_{\mathrm{S}} = -2.15$) portray a slighly different picture of bonding in which the degree of covalency is higher. This suggests that the on-site Coulomb repulsion, which is more accurately modeled by the B3LYP functional, plays an important role in the bonding. The Born effective charges are not consistent with an ionic model based on $Cu^{2+}Fe^{2+}(S^{2-})_2$ which, as mentioned in Sec. I, has been proposed as an explanation for the lower than expected magnetic moment of Fe[10,14].

TABLE II: Comparison of the calculated DFT-B3LYP Born effective charges tensors with those obtained in previous works based on GGA-PW91 calculations by Łazewski *et al.*[19].

Model	Z_{Cu}			Z_{Fe}			Z_{S}		
B3LYP	1.04	-0.04	0.0	2.81	-0.25	0.0	-1.76	0.0	0.0
	-0.04	1.04	0.0	0.25	2.81	0.0	0.0	-2.11	1.12
	0.0	0.0	0.76	0.0	0.0	3.27	0.0	1.03	-2.03
GGA[19]	0.90	0.17	0.0	3.43	-0.21	0.0	-2.12	0.0	0.0
	-0.17	0.90	0.0	0.21	3.43	0.0	0.0	-2.20	1.08
	0.0	0.0	0.46	0.0	0.0	3.80	0.0	1.53	-2.13

In the ground state antiferromagnetic solution, the calculated spin moment of the two Fe atoms in the unit cell are +3.93 and -3.93 μ_{B}. This magnetic configuration is visualized via a plot in which isosurfaces of the spin density is overlayed on top of the optimized unit cell, shown in figure 1b. This confirms that $CuFeS_2$ is antiferromagnetic with spin moments aligned within atomic layers parallel to the crystallograhic a, b plane and opposing along the crystallographic c direction.

The antiferromagnetic state is found to be 0.303 eV per formula unit lower in energy than the fully ferromagnetically coupled state. This is compared with the antiferromagneic-ferromagnetic coupling of 0.445 eV per formula unit calculated by Conejeros *et al.*, who also used the hybrid-exchange B3LYP functional[23]. The discrepancy may be attributable to the different basis sets used in their calculations.

The results presented here are consistent with both experiment and previous theoretical

studies. The calculated (absolute) Fe spin moments of 3.93 μ_B are close to the values of 3.85 μ_B deduced from neutron diffraction measurements by Donnay *et al.*[13] and 3.89 μ_B from DFT-B3LYP calculations by Conejeros *et al.*[23]. The calculated spin moments is less than the value expected for an Fe^{3+} ion (5 μ_B) but it can nevertheless be concluded from examination of the population analysis of individual orbitals that each Fe d-orbital is singly-occupied, which provide support to the Fe^{3+} ($3d^5$) oxidation state. The tetrahedral crystal field results in an unpaired electron occupying each of the two energetically lower e-symmetry states (the spin moment for each orbital is ~0.86 μ_B) and an unpaired electron occupying each of the three energetically higher t_2-symmetry states (the spin moment for each orbital is ~0.70 μ_B). The slight reduction of the spin from 1 μ_B in each orbital is due to hybridization of $3d$-Fe with $2p$-S. No spin is localized on the Cu and S, which again is consistent with the $Cu^+Fe^{3+}(S^{-2})_2$ oxidation state.

The density of states (DOS) (total and that projected onto Cu, Fe and S) of the optimized ground state of $CuFeS_2$ are plotted in Fig. 2. For Fe, the DOS are further projected onto the two individual Fe atoms of the unit cell, labelled "spin-up" and "spin-down" sites. In addition, the DOS contributions from spin-up (α) electrons and spin-down (β) electrons are plotted separately, above (in solid) and below (in dashed) the x-axis respectively. This allows the antiferromagnetic nature of the $CuFeS_2$ ground state to be clearly seen. Centered around an energy of -6.5 eV below the valence band maximum (VBM), there is a highly localized band of $3d$-Fe states which indicate that the Fe-S interactions are strongly ionic. However, these states are somewhat hybridized with $3p$-S states which, as mentioned before, explains the lower magnetic moment compared to what is expected for a purely ionic system. Compared to Fe, the contributions of the valence Cu $3d$-states are spread over several bands between around -5.4 eV and the VBM. The dispersion of the $3d$-Cu states is attributed to covalent interactions with $3p$-S states, apparent in the large degree of overlap of $3d$-Cu and $3p$-S states in the energy range. More evidence of covalent Cu-S interactions can be observed by separating the $3d$-Cu states further into those attributed to t_2 or e orbitals, as seen in Fig. 3. The plot shows that the dispersion of the $3d$-Cu states is mostly due to the spread in the energy levels of the t_2 states, whose corresponding orbitals are pointed in the direction of Cu-S bonds. In summary, analysis of the DOS suggests that the electronic structure of $CuFeS_2$ may be described in a semi-ionic model with localized, ionic, Fe-d-electrons and more covalent Cu-d-S-$2p$ interactions.

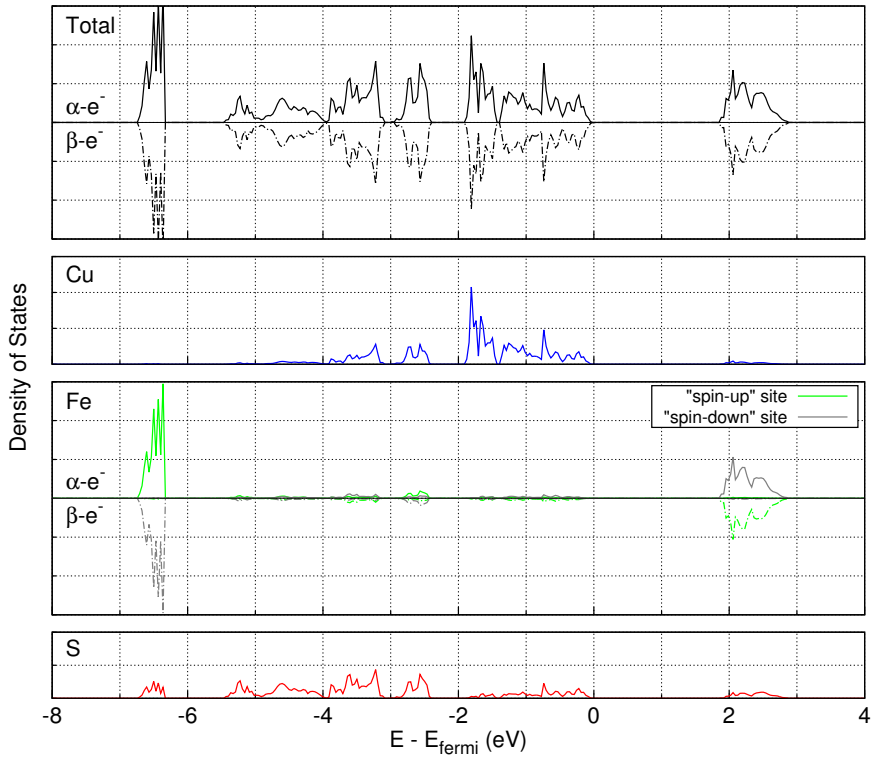


FIG. 2: Density of states (DOS) for the antiferromagnetic ground state solution of $CuFeS_2$. The DOS are also projected onto Cu, Fe and S. For Fe, the DOS are split into contributions from spin-up (α) and spin-down (β) electrons and further projected onto the two invidiual Fe atoms of the unit cell - labelled "spin-up" and "spin-down" site.

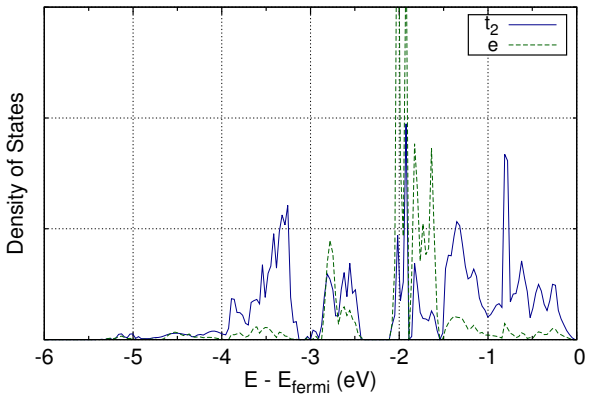


FIG. 3: Density of states (DOS) for $CuFeS_2$ projected onto Cu and split into contributions from t_2 and e orbitals.

The B3LYP band gap estimated from the eigenvalues is 1.82 eV and in disagreement with previous theoretical studies using different treaments of electronic exchange and correlation. LDA calculations performed by Edelbro *et al.* predicted $CuFeS_2$ to be conducting[18] while GGA-PW91 calculations performed by de Oliveira *et al.* predicted $CuFeS_2$ to be a semiconductor with an indirect band gap of 0.1 eV[20]. The estimated band gap here is identical to the B3LYP band gap calculated by Conejeros *et al.*[23]. There is no clear consensus on the measured band gap as discussed in Sec I; band gaps of between 0.33-2.6 eV have been reported[15–17]. As mentioned in Sec II, the B3LYP functional is generally more reliable for estimating the electronic band gap than LDA or GGA, which tend to underestimate the band gap[21].

C. Comparison with Cu_2S and Fe_3S_4

The projected DOS of Cu_2S (top), $CuFeS_2$ (middle), and Fe_3S_4 (bottom) are plotted separately in Fig. 4. For ease of comparison, the $CuFeS_2$ DOS are only projected on one (the "spin-up" site) of the two Fe sites in the unit cell. For Fe_3S_4, the $3d$-Fe DOS are separated into states belonging to type A Fe or type B Fe sites, as described in Sec. II. This allows Fe-S interactions in $CuFeS_2$ and Fe_3S_4 to be compared for Fe of identical oxidation state (Fe^{3+}) and coordination (tetrahedral).

Despite Cu and S being in the same oxidation state (Cu^+; S^{2-}) in both Cu_2S and $CuFeS_2$, the bonding structure of the two compounds is rather different. The optimized crystal structure of Cu_2S is complex; Cu atoms are mostly in triangular coordination with S with Cu-S bonds that vary in length from 2.24 to 2.69 Å with an average length (2.39 Å) similar to the length of Cu-S bonds in $CuFeS_2$ (2.40 Å). In addition, Cu_2S has a more tightly packed crystal structure; each Cu atom is also closely neighbored (separation of between 2.5 and 3.0 Å) to several (between 2 and 5) other Cu atoms while most S atoms are six-fold coordinated to Cu. In the DOS of Cu_2S two valence bands can be identified about the Fermi energy. The upper band between -4.0 eV and the VBM consists of mostly $3d$-Cu states weakly mixed with $3p$-S states while the lower band between 6.5 and 4.2 eV consists of a roughly equal mixture of $3d$-Cu and $3p$-S states. The strong hybridization in the lower valance band suggests that Cu_2S is a semi-ionic compound. As the electronic structure is based on a fully occupied Cu d-band the effects of the on-site Coulomb repulsion are not visible. The overall

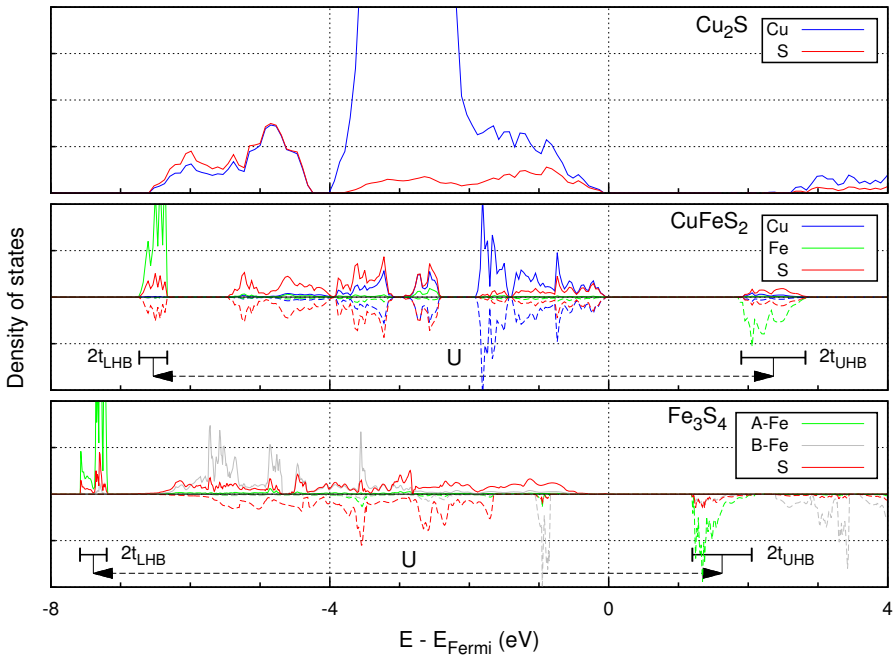


FIG. 4: Projected density of states for $CuFeS_2$, Cu_2S and Fe_3S_4. For $CuFeS_2$ (mid) and Fe_3S_4, the spin up (α) and spin down (β) electrons are plotted above and below the y-axis respectively.

width of the combined valence $3p$-S and $3d$-Cu bands (~6.6 eV) in Cu_2S exceeds that of its counterpart in $CuFeS_2$ (~5.5 eV), which is expected since there is more overlap of valence orbitals in Cu_2S due to its greater Cu-S coordination and shorter bond lengths. Considered in conjunction with the strong hybridization of $3p$-S and $3d$-Cu states in the lower valence band the suggests that the degree of covalency of Cu-S bonds is higher in Cu_2S than in $CuFeS_2$. In summary, Cu-S interactions in Cu_2S and $CuFeS_2$ are similar in the sense that they have a mixed ionic and covalent character despite the different geometric coordination, and the degree of covalency is higher in Cu_2S.

The local structure of type A Fe sites in Fe_3S_4 is similar to that of Fe in $CuFeS_2$. In addition to the Fe in both having tetrahedral coordination, the average type A Fe-S bond length of 2.33 Å is only slighly longer than the average Fe-S bond length in $CuFeS_2$ (2.30 Å). The splitting of the occupied and unoccupied Fe-d-states is due to strong on-site electron correlation. This is typically well described in the B3LYP approximation[31,32,49–51]. The electronic interactions in Fe_3S_4 can be mapped to that of a Hubbard-Anderson Hamiltonian of the form:

$$H = \sum_i \epsilon_i n_{i\sigma} - t \sum_{\langle i,j \rangle \sigma} c^{\dagger}_{i\sigma} c_{j\sigma} + U \sum_i n_{i\uparrow} n_{i\downarrow} \quad (1)$$

where ϵ_i is the energy of an Fe d-orbital, $c^{\dagger}_{i\sigma}$ and $c_{j\sigma}$ are annihilation and creation operators for d electrons of spin σ on Fe lattice sites i and j respectively, U represents the intra-d-electron Coulomb repulsion energy, t is the hopping integral representing the kinetic energy of electrons hopping between atoms, and n_i is the number operator for the site i. In the strong correlation regime ($U >> t$) this produces an (occupied) lower and (unoccupied) upper Hubbard band, each of width $2t$ and separated by an energy U. Examining Figure 4, the lower and upper bands for the tetrahedrally coordinated type A Fe^{3+} site (marked $2t_{LHB}$ and $2t_{UHB}$) are centered at -7.39 and 1.63 eV with widths of 0.38 and 0.85 eV, respectively. This suggests that the electronic structure may be modeled with a U value of 9.02 eV and t value of 0.31 eV (average of t_{LHB} and t_{UHB}).

For $CuFeS_2$, the lower and upper Hubbard bands for $3d$-Fe can be identified centered at around -6.53 and +2.36 eV respectively, implying a U value of 8.89 eV. Their respective bandwidths are 0.40 and 0.92 eV, giving an effective t value of also 0.33 eV. The parameters derived for Fe_3S_4 thus describe the electronic structure of $CuFeS_2$ rather well. The following can therefore be concluded: (1) Further confirmation that Fe in $CuFeS_2$ is in the Fe^{3+} oxidation state is obtained which in turn validates the $Cu^{+}Fe^{3+}(S^{2-})_2$ oxidation state. (2) The nature of Fe-S bonding in $CuFeS_2$ and Fe_3S_4 (for type A Fe) is very similar and essentially ionic. (3) In both cases the electrons of the Fe^{3+} site are highly localized and strongly correlated, corresponding to the $U >> t$ regime in the Hubbard-Anderson model. It should be noted that the Hubbard U values deduced here are only indirectly related to that of the widely used DFT+U approaches. In the GGA+U approach employed for bulk $CuFeS_2$ by Zhou *et al.*[44], they determined an optimal U parameter of 3 eV, which is significantly different to the one determined here from the DOS.

IV. CONCLUSIONS

A hybrid-exchange density functional study of the geometry and electronic structure of states of bulk $CuFeS_2$ has been presented. The calculated optimized structure of the chalcopyrite has lattice parameters and bond lengths in agreement with those measured

with a slight overestimation of around 3%. The ground state of $CuFeS_2$ is found to be antiferromagnetic, agreeing with previous calculations and experiments. Analysis of the electronic structure through the projected density of states and spin moments reveals a mixtured picture of bonding where the Fe^{3+} sites are strongly ionic while Cu^{+} sites are semi-ionic and engage in covalent interactions with S^{2-} ligands. The slight hybridization of $3d$-Fe and $3p$-S states accounts for the lower than expected spin density of the d^5 Fe^{3+}. The calculated band gap of 1.8 eV is within the range of published experimental values and is likely to be more accurate than previous calculations using LDA or GGA functionals due to the use of the hybrid-exchange B3LYP functional, in the current study.

In comparison with Cu_2S, which adopts a significantly different bonding structure compared with $CuFeS_2$, it was found that Cu-S interactions in both materials are semi-ionic but with a higher degree of covalency in Cu_2S. Conversely, the properties of type A Fe^{3+} sites in Fe_3S_4 was found to close match that of $CuFeS_2$ Fe^{3+} sites, both in terms of the local geometry and electronic structure. For the latter, remarkably similar on-site repulsion (U~8.9 eV) and hopping integral (t~0.3 eV) values were deduced for $CuFeS_2$ and Fe_3S_4 when their $3d$-Fe states were mapped to the Hubbard-Anderson model. It can be concluded from analysis of the electronic structure and spin density in addition to the comparison with Cu_2 and Fe_3S_4 that $CuFeS_2$ is best modeled using the oxidation state $Cu^{+}Fe^{3+}(S^{2-})_2$ and that both strong electronic correlation and covalent interactions play an important in the bonding.

V. ACKNOWLEDGEMENTS

R.M.-C. thanks the Ministerio de Ciencia e Innovación (Spain) for a 'Juan de la Cierva' Research Contract. V.H.-Y.C. was supported through a studentship in the Centre for Doctoral Training on Theory and Simulations of Materials at Imperial College London, funded by the Engineering and Physical Sciences Research Council (EPSRC) of the United Kingdom under Grant No. EP/G036888/1. This work was supported by the Rio Tinto Centre for Advanced Mineral Recovery at Imperial College London.

REFERENCES

[1]A. Jager-Waldau, Sol. Energ. Mat. Sol. Cells **95**, 1509 (2010).

[2]J. L. Shay and J. H. Wernick, *The science of the solid state*, Vol. 7 (Pergamon Press, New York, 1975).

[3]R. C. Smith, Journal de Physique **36**, 89 (1975).

[4]P. Migliorato, B. Tell, J. L. Shay, and H. M. Kasper, Appl. Phys. Lett. **24**, 227 (1971).

[5]N. A. Goryunova, A. V. Anshon, I. A. Karpovich, E. I. Leonov, and V. M. Orlov, Phys. Status Solidi (a) **2**, K117 (1970).

[6]G. A. Medvedkin, T. Ishibashi, T. Nishi, K. Hayata, Y. Hasegawa, and K. Sato, Jpn. J. Appl. Phys. **39**, L949 (2000).

[7]Y.-J. Zhao, P. Mahadevan, and A. Zunger, Appl. Phys. Lett. **84**, 3753 (2004).

[8]D. F. Marrón, A. Martí, and A. Luque, Thin Solid Films **517**, 2452 (2009).

[9]Y. Cai, X. Chen, J. Ding, and D. Zhou, Hydrometallurgy **113-114**, 109 (2012).

[10]L. Pauling and L. O. Brockway, Z. Kristallogr. **82**, 188 (1932).

[11]C. L. Burdick and J. H. Ellis, J. Am. Chem. Soc. **39**, 2518 (1917).

[12]V. V. Popov, S. A. Kizhaev, and Y. V. Rud, Phys. Solid State **53**, 71 (2011).

[13]G. Donnay, L. M. Corliss, J. D. H. Donnay, N. Elliott, and J. M. Hastings, Phys. Rev. **112**, 1917 (1958).

[14]C. Kurylenko, Bull. Soc. Franc. Mineral. Cristallogr. **65**, 59 (1942).

[15]I. G. Austin, C. H. L. Goodman, and A. E. Pengelly, J. Electrochem. Soc. **103**, 609 (1956).

[16]T. E. Engin, A. V. Powell, and S. Hull, J. Solid State Chem. **184**, 2272 (2011).

[17]T. Teranishi, J. Phys. Soc. Japan **16**, 1881 (1961).

[18]R. Edelbro, A. Sandström, and J. Paul, Appl. Surf. Sci. **206**, 300 (2003).

[19]J. Łazewski, H. Neumann, and K. Parlinski, Phys. Rev. B **70**, 195206 (2004).

[20]C. de Oliveira and H. A. Duarte, Appl. Surf. Sci. **257**, 1319 (2010).

[21]J. Muscat, A. Wander, and N. M. Harrison, Chem. Phys. Lett. **342**, 397 (2001).

[22]K. G. Nikiforov, Prog. Cryst. Growth Charact. **39**, 1 (1999).

[23]S. Conejeros, P. Alemany, M. Llunell, I. de P. R. Moreira, V. Sánchez, and J. Llanos, Inorg. Chem. **54**, 4840 (2015).

[24]R. Dovesi, V. R. Saunders, C. Roetti, R. Orlando, C. M. Zicovich-Wilson, F. Pascale, B. Civalleri, K. Doll, N. M. Harrison, I. J. Bush, P. D'Arco, and M. Llunell, *CRYSTAL09 User's Manual* (2009).

[25]K. Doll and N. M. Harrison, Chem. Phys. Lett. **317**, 282 (2000).

[26]M. Catti, G. Valerio, and R. Dovesi, Phys. Rev. B **51**, 7441 (1995).

[27]P. Azavant and A. Lichanot, Acta Cryst. **A49**, 91 (1993).

[28]A. D. Becke, J. Chem. Phys. **98**, 5648 (1993).

[29]C. Lee, W. Yang, and R. G. Parr, Phys. Rev. B **37**, 785 (1988).

[30]D. Muñoz, N. M. Harrison, and F. Illas, Phys. Rev. B **69**, 085115 (2004).

[31]X. Feng and N. M. Harrison, Phys. Rev. B **69**, 035114 (2004).

[32]X. Feng and N. M. Harrison, Phys. Rev. B **69**, 132502 (2004).

[33]N. C. Wilson, J. Muscat, D. Mkhonto, P. E. Ngoepe, and N. M. Harrison, Phys. Rev. B **71**, 075202 (2005).

[34]L. Pisani, R. Valenti, B. Montanari, and N. M. Harrison, Phys. Rev. B **76**, 235126 (2007).

[35]G. Mallia and N. M. Harrison, Phys. Rev. B **75**, 165201 (2007).

[36]G. C. De Fusco, L. Pisani, B. Montanari, and N. M. Harrison, Phys. Rev. B **79**, 085201 (2009).

[37]S. Tomić, L. Bernasconi, B. G. Searle, and N. M. Harrison, J. Phys. Chem. C **118**, 14478 (2014).

[38]S. Tomić, B. Montanari, and N. M. Harrison, Physica E: Low-dimensional Systems and Nanostructures **40**, 2125 (2008), 13th International Conference on Modulated Semiconductor Structures.

[39]N. C. Wilson and J. Muscat, Mol. Sim. **28**, 903 (2001).

[40]C. Pisani, R. Dovesi, and C. Roetti, *Hartree-Fock ab initio Treatment of Crystalline Systems*, Lecture Notes in Chemistry, Vol. 48 (Springer Verlag, Heidelberg, 1988).

[41]S. W. Goh, A. N. Buckley, R. N. Lamb, R. A. Rosenberg, and D. Moran, Geochim. Cosmochim. Acta **70**, 2210 (2006).

[42]A. R. Lennie, S. A. T. Redfer, P. E. Champness, C. P. Stoddart, P. F. Schofield, and D. J. Vaughan, Am. Mineral. **82**, 302 (1997).

[43]M. Uda, Am. Mineral. **50**, 1487 (1965).

[44]M. Zhou, X. Gao, Y. Cheng, X. Chen, and L. Cai, Appl. Phys. A **118**, 1145 (2015).

[45]T. Kratz and H. Fuess, Z. Kristallogr. **186**, 167 (1989).

[46]J. Paier, M. Marsman, and G. Kresse, J. Chem. Phys. **127**, 024103 (2007).

[47]M. Marsman, J. Paier, A. Stroppa, and G. Kresse, J. Phys.: Condens. Matter **20**, 064201 (2007).

[48]R. D. King-Smith and D. Vanderbilt, Phys. Rev. B **47**, 1651 (1993).

[49]W. Wu, A. J. Fisher, and N. M. Harrison, Phys. Rev. B **84**, 024427 (2012).

[50]S. Muhkopadhyay, M. W. Finnis, and N. M. Harrison, Phys. Rev. B **87**, 125132 (2013).

[51]G. C. D. Fusco, B. Montanari, and N. M. Harrison, Phys. Rev. B **82**, 220404 (2010).